Chemical Science

Dynamic Article Links ▶

Cite this: DOI: 10.1039/c0xx00000x

www.rsc.org/xxxxxx

EDGE ARTICLE

Electronic Supplementary Information

Rotationally inelastic scattering of CD_3 and CH_3 with He: comparison of velocity map-imaging data with quantum scattering calculations

Ondřej Tkáč,[a] Alan G. Sage,[a] Stuart J. Greaves,[b] Andrew J. Orr-Ewing,*[a] Paul J. Dagdigian,*[c] Qianli Ma[c] and Millard H. Alexander[d]

Received (in XXX, XXX) Xth XXXXXXXXX 20XX, Accepted Xth XXXXXXXXX 20XX
DOI: 10.1039/b000000x

Experimental parameters and angular resolution

Figure S1 shows the dependence of calculated angular resolution for the CD_3 + He scattering system on the CM-frame scattering angle. Total angular resolution is given by the contribution from the velocity spread and angular divergence of the beams. The angular resolution is calculated for the transition from $n_k = 1_1$ to $n'_{k'} = 2_1$. For example, the angular resolution is shown to be ~12º for a scattering angle θ = 90º, which means that molecules scattered into θ = 90º in the CM frame will be distributed over a 12º angular range in the ion-image. This spread of angles results from superposition of many Newton spheres differing slightly in the magnitude and direction of the initial velocities of the collision partners. For the limiting case of an angular resolution of 0º, all molecules scattered into a given CM-frame angle would be mapped onto the same angle in the ion image. The degradation of resolution in the images is in the angular rather than the radial coordinate, so changes in resolution are difficult to see by eye. A comparison of total angular resolution for CD_3 scattered with He into the final states $n'_{k'} = 2_1$ and 5_5 is shown in Fig. S2. The angular resolution is poorer for inelastic scattering leading into the final state $n'_{k'} = 5_5$. This can be understood by realizing that the larger energy transfer connected with a higher final rotational energy level results in a smaller Newton sphere.

Figure S3 shows experimental and simulated REMPI spectra of CD_3 radicals, with the experimental sample prepared jet-cooled in the primary molecular beam of the crossed molecular beam apparatus under the conditions employed for inelastic scattering experiments. The CD_3 radicals were formed by 266-nm photolysis of CD_3I seeded in Ar, close to the orifice of the pulsed nozzle used to generate the molecular beam. By selective integration of ion signals at the position-sensitive detector, only radicals created by the photolysis laser in the nozzle expansion region (and not those from photolysis of CD_3I by the probe laser in the centre of the CMB apparatus) contributed to this spectrum. The intense peak corresponding to the *Q*-branch goes off-scale. Several peaks of the *O*, *P*, *R* and *S* branch structure are assigned.

A rotational temperature of 15 K in the PGOPHER simulations best reproduced the pattern of intensities in the (non

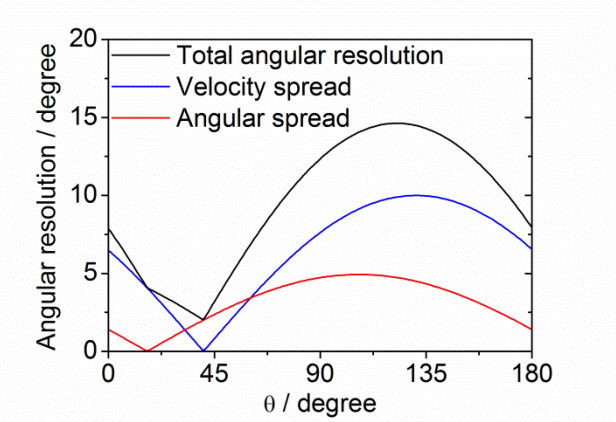

Figure S1 The total angular resolution of the CD_3+ He scattering system (black line) at a collision energy of 440 ± 35 cm^{-1}. The experimental reesolution is reduced by the velocity and angular spread of the molecular beams, as shown by the blue and red lines respectively. The angular resolution is calculated for the transition from $n_k = 1_1$ to $n'_{k'} = 2_1$.

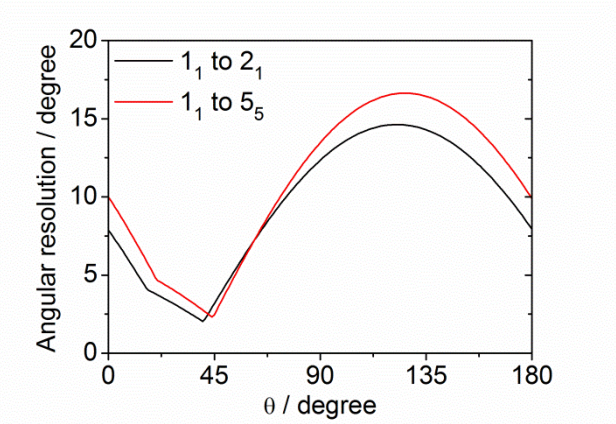

Figure S2 The total angular resolution of the CD_3+ He system for CD_3 final states $n'_{k'} = 2_1$ and 5_5 at a collision energy of 440 ± 35 cm^{-1}.

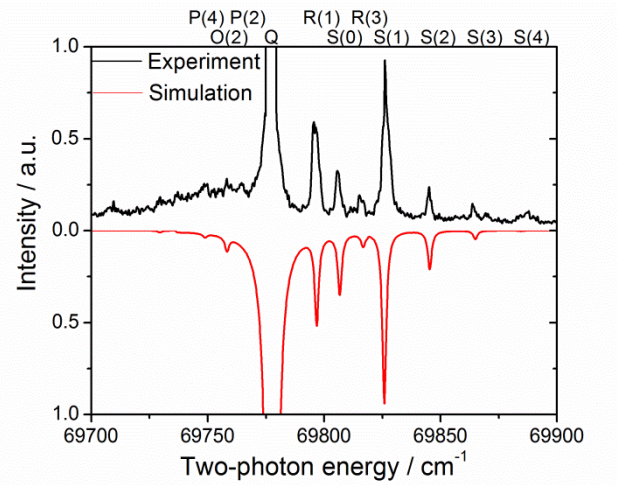

Figure S3 Experimental and simulated (2+1) REMPI spectra of the jet-cooled CD_3 radicals produced by 266 nm photolysis of CD_3I in a nozzle expansion. The REMPI spectra employ the $4p^2A_2'' \leftarrow \tilde{X}^2A_2''$ 2-photon transition.

Q-branch) spectral lines observed in this and other experimental spectra. The simulations incorporate the effect of nuclear spin statistics, calculated for a room-temperature sample, and we assume there is no conversion between populations of different nuclear spin states as the radicals cool in the supersonic expansion. The CD_3 radical has population in the individual nuclear spin modifications in the ratio $A_2 : A_1 : E = 1 : 10 : 16$. At a rotational temperature of 0 K the entire population would be in the lowest rotational levels corresponding to each individual nuclear spin modification [0_0 (3.70%), 1_0 (37.0%), 1_1 (59.3%)]. For the CH_3 radical, the populations in the A_2 and E nuclear spin modifications are 1:1, and at a rotational temperature of 0 K only the 0_0 and 1_0 levels would be (equally) populated.

The speeds of the molecular beams were determined from the centres of the CD_3 images from photodissociation of CD_3I entrained in both primary and secondary molecular beams, since the centre of mass velocity of the Newton sphere corresponds to the velocity of the molecular beam. The measured beam velocities were $v_{CD_3} = 550 \pm 30$ m s^{-1} and $v_{He} = 1710 \pm 80$ m s^{-1} (with the uncertainties representing $\pm$HWHM of the speed distributions). The angular divergence distributions and spatial widths of the two molecular beams were calculated from the geometrical arrangement, using known nozzle and skimmer diameters and nozzle-to-skimmer and skimmer-to-scattering-centre distances. The temporal profiles of the molecular beams were measured by changing the delay time between opening of the nozzles and firing of the probe laser and measuring the unscattered CD_3 radical signal. The FWHM of each measured distribution was then used in the Monte Carlo simulation program for density-to-flux conversion, and to derive the angular resolution of the experiment and its dependence on CM-frame scattering angle.

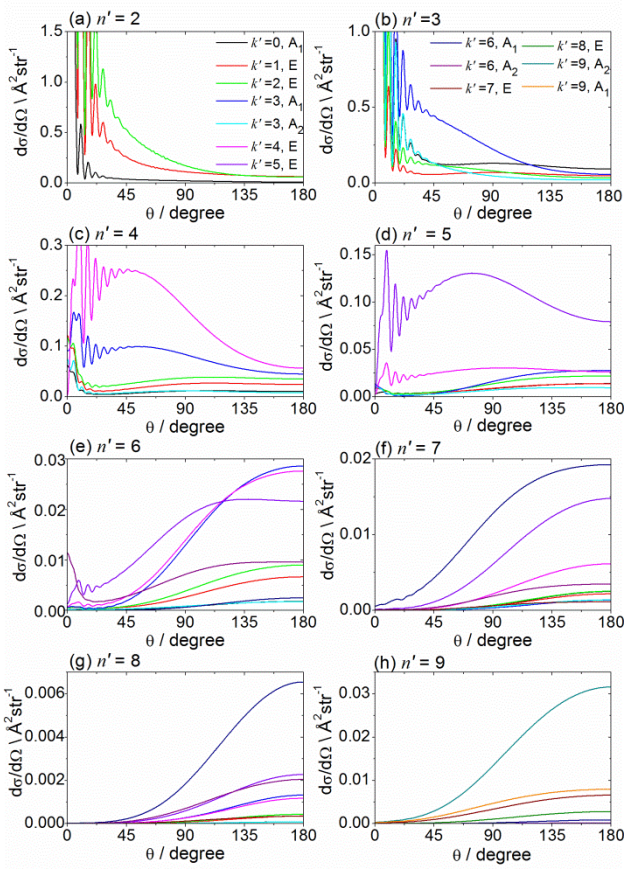

Figure S4 Theoretical DCSs for CD_3 + He scattering at a mean collision energy of 440 cm^{-1}, calculated for individual k' projection levels of the CD_3 final level for $n' = 2$ - 9. The initial level is a weighted average over the distribution of populations of the levels present in the molecular beam (Table 1). The legend shown in panels (a) and (b) is valid for all (a) – (h).

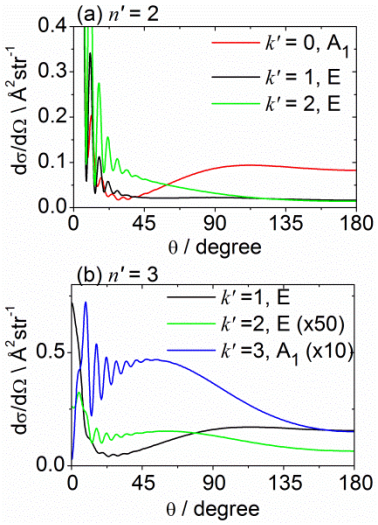

Figure S5 Theoretical DCSs for CH_3 + He scattering at a mean collision energy of 425 cm^{-1}, calculated for individual k' projection levels of the CH_3 final level for $n' = 2$ and 3. The initial level is a weighted average over the distribution of populations of the levels present in the molecular beam (Table 1).

Computed single-state-resolved differential cross sections

Even though the DCSs for individual k' projection levels of a given n' quantum number of the final scattering level are not accessible by experiment, such DCSs fully resolved in the k' quantum number may be calculated theoretically. Such theoretical $n'_{k'}$-resolved DCSs for $n' = 2 - 9$ and all individual k' projection levels are shown in Fig. S4. The initial levels used in calculating these DCSs are averaged over the population of levels present in our parent beam (Table 1 of the main paper). A similar analysis for CH_3 + He scattering is presented in Fig. S5.

Summing of single-state-resolved differential cross sections

The DCSs were calculated for each $n'_{k'}$ final level, assuming the initial normalized population in the beam (see Table 1). To compute the DCS for a given n' level detected on a specific line, these $n'_{k'}$ DCSs were summed and weighted by the 2-photon line strength factors $S_{k'}$ and then divided by the sum of these 2-photon line strength factors:

$$\frac{d\sigma}{d\Omega} = \frac{\sum_{k'} \frac{d\sigma}{d\Omega}_{k'} S_{k'}}{\sum_{k'} S_{k'}}, \qquad \text{(S1)}$$

Here, the sums run over all k' projection quantum numbers detected for a given n' level on the chosen spectral line.

Further comparisons of differential cross sections

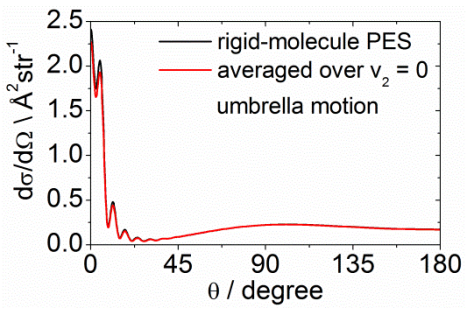

Figure S6 Theoretical DCSs for CD_3 + He scattering for the $1_0 \rightarrow 3_3$ transition calculated using the rigid-molecule PES and a PES in which the umbrella motion was averaged over the $v_2 = 0$ probability distribution.

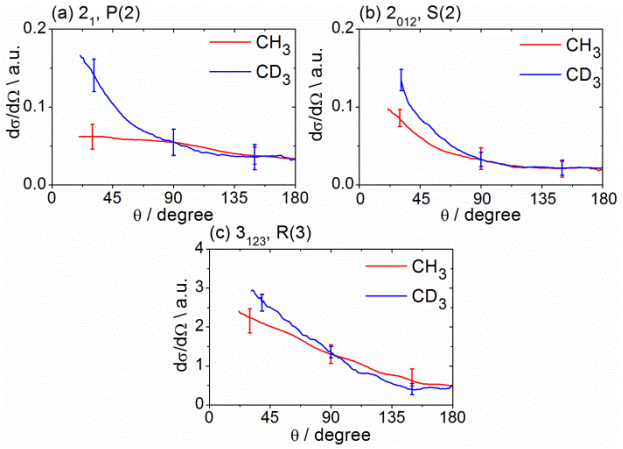

Figure S7 Comparison of experimental DCSs for CD_3 and CH_3. DCSs are normalized to have equal values at $\theta = 90°$.

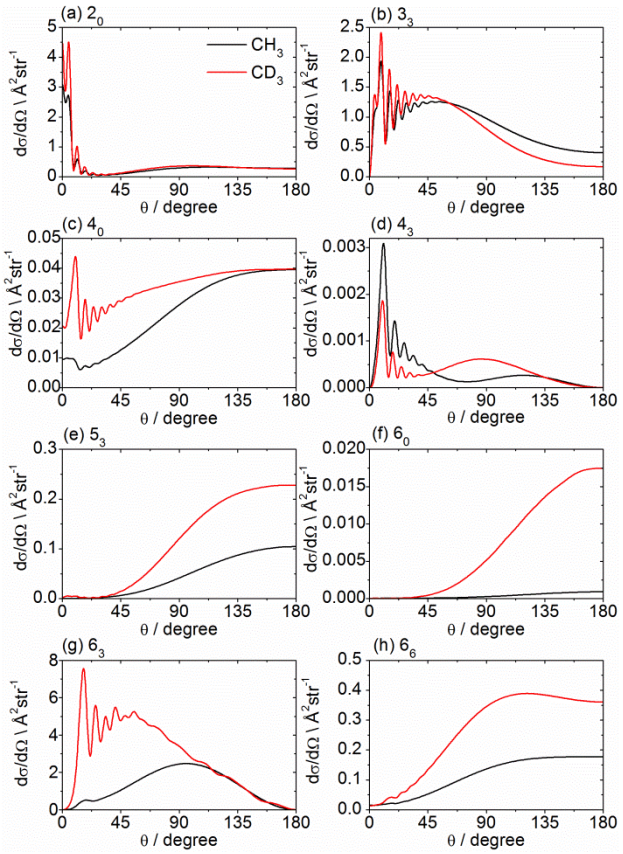

Figure S8 Theoretical state-to state DCSs for inelastic scattering of CH_3 and CD_3 with He out of the $n_k = 0_0$ rotational level, at respective collision energies of 425 and 440 cm^{-1}.

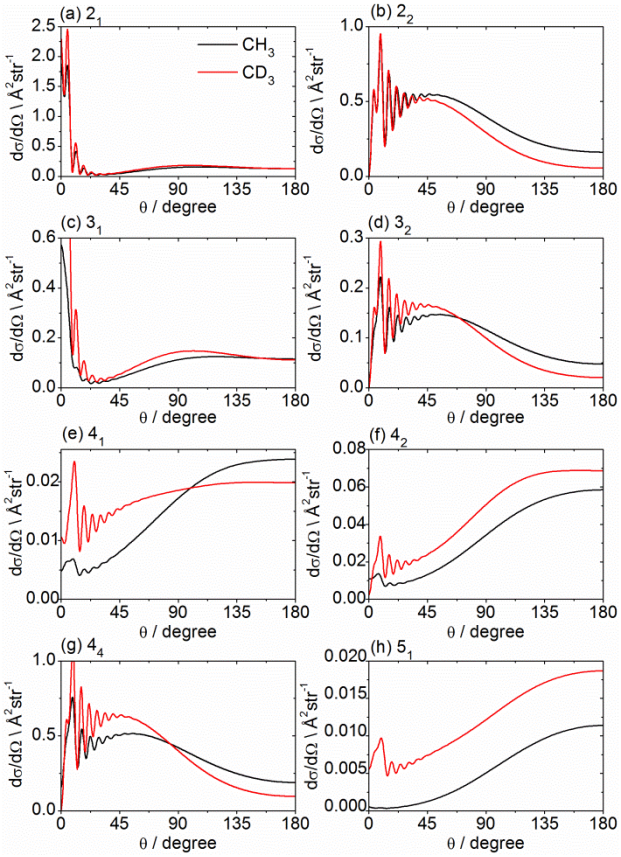

Figure S9 Theoretical state-to state DCSs for inelastic scattering of CH_3 and CD_3 with He out of the $n_k = 1_1$ rotational level, at a collision energy of 425 and 440 cm^{-1}.

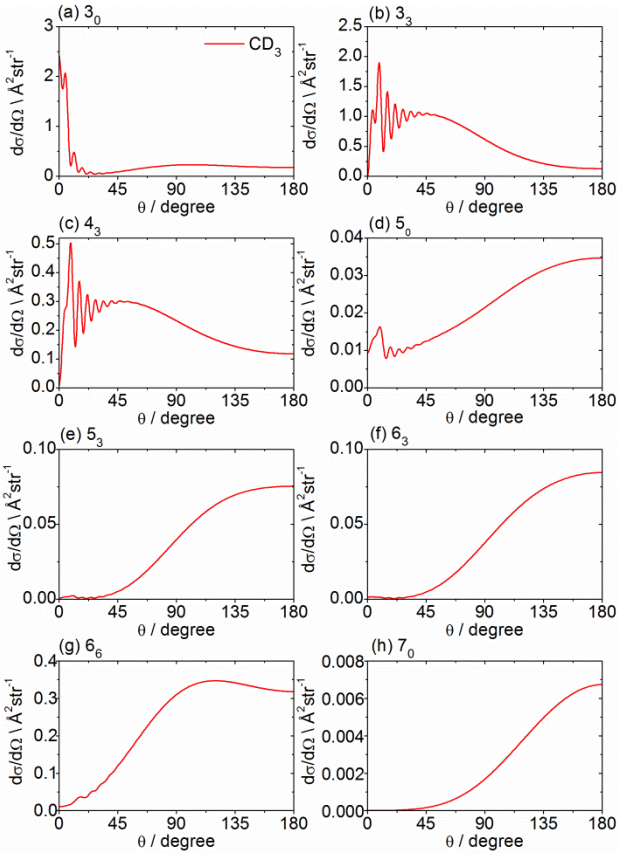

Figure S10 Theoretical state-to state DCSs for inelastic scattering of CD_3 with He out of the $n_k = 1_0$ rotational level, at a collision energy of 440 cm^{-1}. The $n_k = 1_0$ rotational level does not exist for the CH_3 isotopologue.

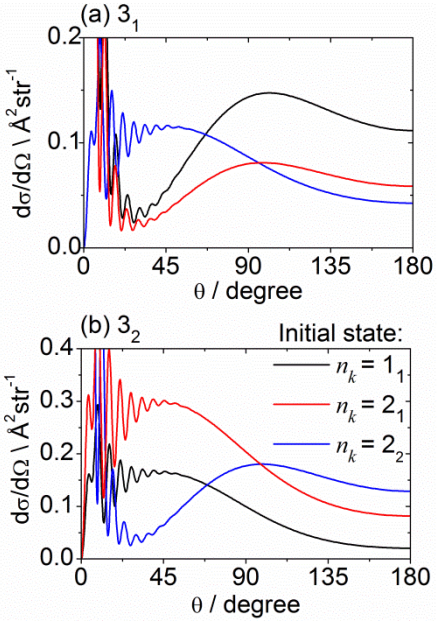

Figure S11 Theoretical state-to state DCSs for inelastic scattering of CD_3 with He out of various initial rotational levels into levels with $n' = 3$, at a collision energy of 440 cm^{-1}.

[a] *School of Chemistry, University of Bristol, Cantock's Close, Bristol BS8 1TS, UK. E-mail: a.orr-ewing@bris.ac.uk*
[b] *School of Engineering and Physical Sciences, Heriot-Watt University, Edinburgh, EH14 4AS UK.*
[c] *Department of Chemistry, The Johns Hopkins University, Baltimore, Maryland 21218-2685, USA. E-mail: pjdagdigian@jhu.edu*
[d] *Department of Chemistry and Biochemistry and Institute for Physical Science and Technology, University of Maryland, College Park, Maryland 20742-2021, USA. E-mail: mha@umd.edu*